JOURNAL OF AIRCRAFT
Vol. 43, No. 2, March–April 2006

General Aviation Propeller–Airframe Integration Simulations

J. Mark Janus*
Mississippi State University, Mississippi State, Mississippi 39762

The interference flowfields of propellers when installed on general aviation aircraft is investigated. The interaction is known to be a significant source of cabin noise and is likely an efficiency loss mechanism due to standard blade designs not completely accounting for installation interference. The aerodynamic model used in the simulations incorporates state-of-the-art unsteady three-dimensional Navier–Stokes solutions through the use of a high-resolution approximate Riemann solver utilizing the Baldwin–Lomax turbulence model. The software used for simulation purposes is a derivative of a software package developed for NASA John. H. Glenn Research Center at Lewis Field. Several configurational arrangements were studied and compared to one another. The propellers tested include a standard general aviation propeller and a modern propeller design. Both are mounted on various fuselage configurations including geometries involving engine cooling inlets and short and long spinners to adjust propeller/cowl spacing. A detailed examination of flowfield properties provides insight into the interaction between the propeller and the cowl immediately downstream.

Nomenclature

C_{pw}	=	power coefficient, $(P/\rho n^3 D^5)$
C_t	=	thrust coefficient, $(T/\rho n^2 D^4)$
c	=	blade station chord, ft
D	=	blade diameter, ft
J	=	advance ratio, (V/nD)
M_{rel}	=	blade-relative Mach number
n	=	blade rotational speed, revolutions per second
P	=	power, ft · lbf/s
p_0	=	total pressure, lbf/in^2 (absolute)
$p_{0\infty}$	=	freestream total pressure, lbf/in^2 (absolute)
R	=	blade tip radius, ft
r	=	blade station radius, ft
T	=	thrust, lbf
V_∞	=	freestream velocity, ft/s
x	=	blade station chordwise direction, ft
α	=	blade-relative angle of attack, deg
β	=	local flow angle, deg
η	=	propeller efficiency (JC_t/C_{pw})
θ	=	reference blade position, deg
ρ	=	fluid mass density, slug

Introduction

THE development of the capability to numerically model the flowfield about rotating configurations has enabled the application of state-of-the-art computational fluid dynamics (CFD) in the analysis and design of general aviation propellers. NASA funded a study to assess the feasibility of using aerodynamic and centrifugal loads on a general aviation propeller to cause blade deflections (changes in pitch) to improve efficiency throughout the flight envelope, in effect creating a quasi-constant speed flexible composite propeller. The study presented here was an aid to that effort to develop an enhanced blade design through the use of CFD for conceptual design testing.

The software used in this study is a derivative of a software package developed for NASA John H. Glenn Research Center at Lewis Field, referred to as the TURBO[1,2] code. Specific software modifications were made to accommodate the propeller–airframe interaction problem at hand, yielding a new software tool referred to as the propeller performance simulator (PROPS) code. The aerodynamic model used in this study incorporates a state-of-the-art unsteady three-dimensional Navier–Stokes solver, discretized as a finite volume method, utilizing a high-resolution approximate Riemann solver for cell interface flux definitions. The numerical scheme is an approximately factored, block LU, implicit, Newton iterative-refinement method. Multiblock domain decomposition is used to partition the field axially and azimuthally into an ordered arrangement of blocks, which exhibit varying degrees of similarity. Block–block relative motion is achieved in the axial direction using an interpolated sliding interface. Block–block interfaces, including dynamic interfaces, are treated to mimic cell communication interior to a block.

A number of configurations were investigated in this study. The configurations studied involve two-bladed propellers, namely, a McCauley design and a conceptual design called the quasi-constant speed (QCS04) propeller. To study the propellers-installed performance, the fuselage of a general aviation trainer aircraft, the Global Aircraft GT3 (with and without cooling inlets) and a body of revolution assembly derived from the equivalent cross-sectional area of the GT3 aircraft cowl were incorporated into the geometries modeled. All simulations were performed using uniform inflow conditions. Data collected from the numerical solutions included aerodynamic force and moment coefficients on the blades, integrated performance parameters, and flowfield maps. Typically, the results are displayed in the form of shaded (or contoured) pressure plots, integrated surface measurables, and calculated propeller performance parameters.

The research interest centered around the unsteady analysis of the flow about a propulsive device in its installed configuration. Although some measures are taken to account for interference effects when designing a propeller, volumes can be learned from a virtual installation using computational tools. In this regard, the present work is considered to be a nontrivial research effort having to do with the computation of the three-dimensional unsteady flow simulating the installed performance of various complex rotating configurations.

Simulation Model

The approach taken in the present work is to use computational tools that were developed for the numerical solution of rotating machinery problems on dynamic multiblock grids.[1–6] This effort uses computational techniques and experience gained in computing unsteady flows about complex geometries using dynamic multiblock grids. The flow solver and dynamic multiblock grid approach are based on earlier work with some development for this new

Presented as Paper 2000-0357 at the 38th Aerospace Sciences Meeting & Exhibit, Reno, NV, 10–13 January 2000; received 1 January 2005; revision received 4 April 2005; accepted for publication 5 April 2005.

*Associate Professor, Department of Aerospace Engineering, Computational Simulation and Design Center, Box 9627. Senior Member AIAA.

propeller–airframe configuration. The baseline code, TURBO, has been through an extensive validation process. One purpose of this effort has been to demonstrate the utility of the extended software tool (PROPS) by its application toward the simulation of the unsteady flow about complex propeller–airframe integration configurations and to compare the resulting numerical solutions.

Simulation Results

GT3 Plus McCauley Analysis

The first comparison is between 1) the GT3 fuselage with a McCauley propeller at cruise conditions, shown in Fig. 1, and 2) an equivalent area cowl (EAC) with the McCauley propeller, shown in Fig. 2. For reference purposes, the blade positions discussed are shown in Fig. 1; also the location of the GT3 cooling inlets are shown in Fig. 1 but were not active for this first comparison. The grid used this study utilized two blade rows. The forward blade row contained the McCauley blade and the aft blade row contained the GT3 fuselage. The simulated design cruise condition for the GT3 was a flow velocity of 110 knots indicated airspeed (KIAS) at sea level with the propeller operating at 2710 rpm. As mentioned in the Introduction, the flowfield communication between the rotating forward row and the stationary aft row was accomplished via a sliding interpolated interface. The grid sizes were $62 \times 39 \times 80$ (axial $\times$ radial $\times$ circumferential cells) for the forward row, and $64 \times 39 \times 80$ (axial $\times$ radial $\times$ circumferential cells) for the aft row. Grid refinement was used to maintain $y^+ < 10$. The solutions presented were monitored for periodicity and are after 5+ blade revolutions. Subiterations were used at each time step in an effort to maintain unsteady accuracy.

The mean efficiency for the GT3 plus McCauley case was compared to the efficiency vs advance ratio data obtained for the EAC plus McCauley case. The time-dependent total propeller efficiency, that is, accounting for both blades, shown in Fig. 3, was made by sampling the data periodically as the propeller rotated through one complete clockwise revolution. Tracking was made by noting the position of a reference blade, which began at $\theta = 0$ deg. The data for the GT3 case were then time averaged for comparison to the EAC data, as shown in Fig. 4. The maximum and minimum values of total propeller efficiency for the GT3 case are also indicated using error bars in Fig. 4. A drop in mean efficiency of nearly 10% is evident for the GT3 configuration, which is apparently due to the nonaxisymmetric shape of the fuselage immediately downstream.

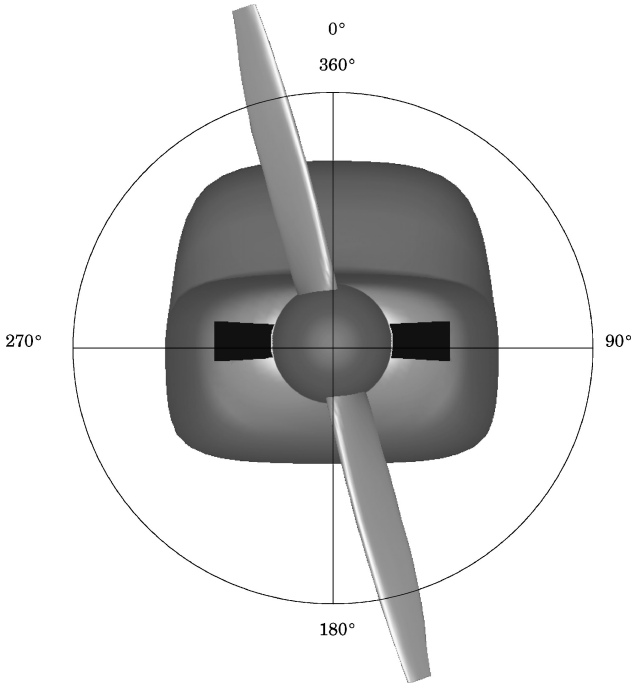

Fig. 1 GT3 fuselage plus McCauley propeller with cooling inlets.

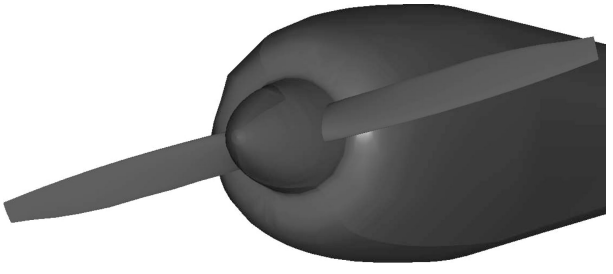

Fig. 2 EAC plus McCauley propeller.

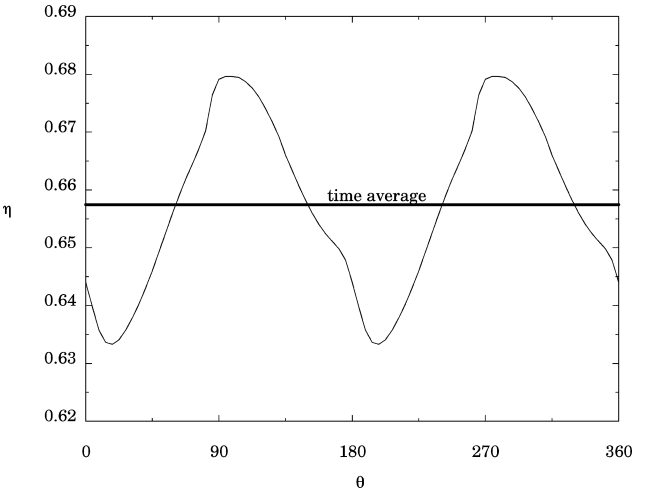

Fig. 3 Time-dependent total propeller efficiency.

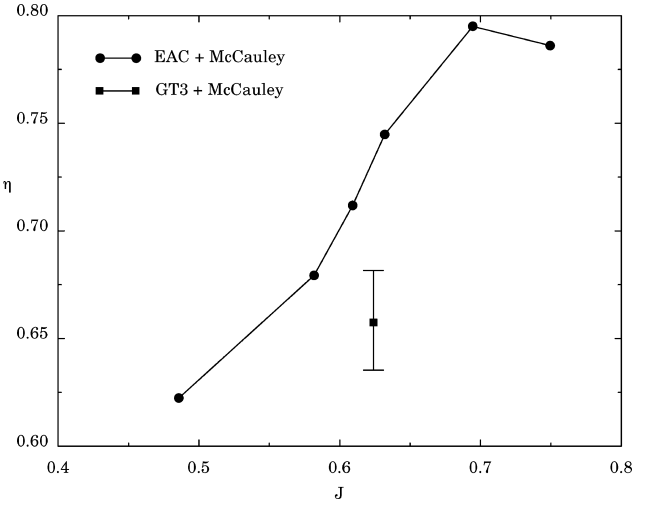

Fig. 4 GT3 vs EAC efficiency comparison.

In an effort to make this analysis more realistic, the GT3 configuration was also simulated with cooling inlets, as shown in Fig. 1. The cooling inlets were simulated using an outflow boundary condition, where a pressure could be specified to control the flow rate into the passages. A flow rate consistent with the cooling requirement of a typical general aviation engine was selected. The fuselage interference effects were then compared with and without cooling inlet flow.

A cruise condition comparison of the GT3 plus McCauley time-dependent relative angle of attack vs azimuthal position was made at selected radial locations to demonstrate the nonuniform (blade) inflow conditions set up by a nonaxisymmetric cowl. First, the time-dependent flow angle was determined by initially locating the forwardmost stagnation point. The flow angle was taken at a location outside the boundary layer roughly normal to the local surface at this point.

Significant variation in flow angle is seen by the blade, as shown in Fig. 5, which shows the flow angle relative to the axis of rotation

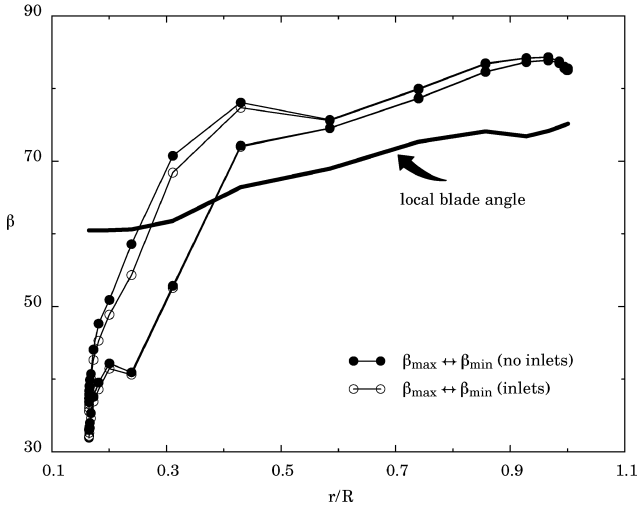

Fig. 5 Approaching flow angle envelope (relative to the axis of rotation): GT3, $V_\infty = 110$ KIAS, sea level, McCauley, 2710 rpm.

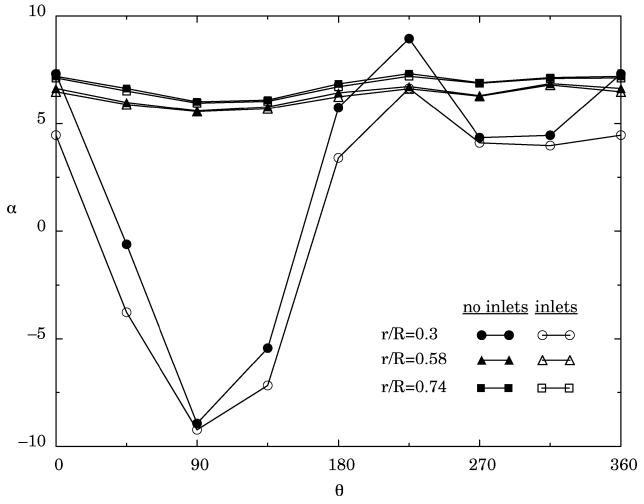

Fig. 6 Time-dependent blade-relative angle of attack: GT3, $V_\infty = 110$ KIAS, sea level, McCauley, 2710 rpm.

for the configuration with and without cooling inlets. The pair of curves in Fig. 5 for each configuration show the maximum flow angle (upper curve) and the minimum flow angle (lower curve) seen at different radial stations during a complete revolution. In the vicinity of the fuselage, the flow angle is shown to vary significantly. The variation is also highlighted in Fig. 6 as blade-relative angle of attack vs azimuthal position of the blade. The blade-relative angle of attack was determined by referencing the flow angle to the local blade angle shown in Fig. 5.

The data in Figs. 5 and 6 give an indication that the root portion of the blade is operating at a fairly large negative angle of attack. The vector field shown in Fig. 7 shows a representative blade-relative velocity at a radial position near the root of the blade ($r/R = 0.22$), with the propeller blade in the vertical position ($\theta = 0$ deg). The local operation of the blade at such an angle of attack will have an adverse effect on the total propeller efficiency.

GT3 Plus QCS Analysis

In addition to the installed-performance simulations of the McCauley propeller with the GT3 fuselage and the EAC, similar simulations were performed for the QCS04 propeller design shown in Fig. 8 with the GT3 fuselage. The design of the QCS04 blade accounted for the fuselage interference flowfield by suitably adjusting the blade twist in the vicinity of the hub and fuselage engine cowl.

As with the earlier configuration, the grid used in the study of the QCS04 incorporated two blade rows. The forward blade row

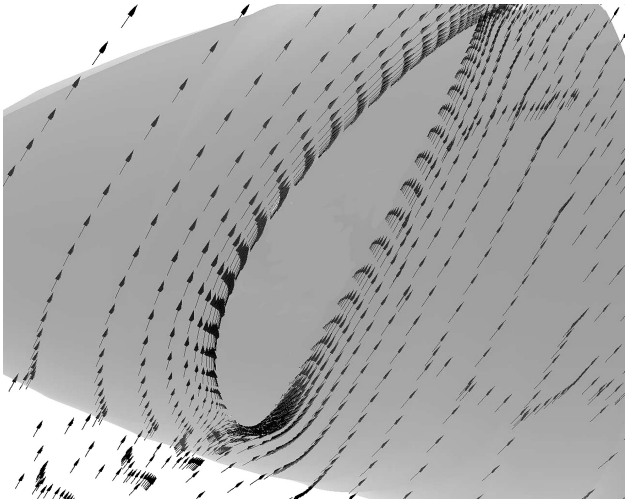

Fig. 7 Blade-relative velocity vectors ($r/R = 0.22$).

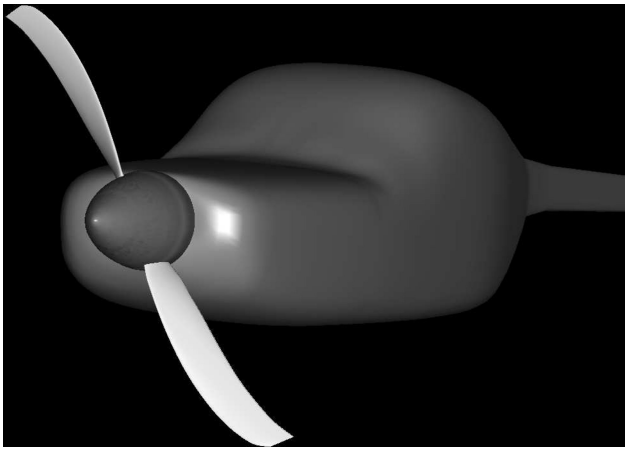

Fig. 8 GT3 fuselage with QCS propeller.

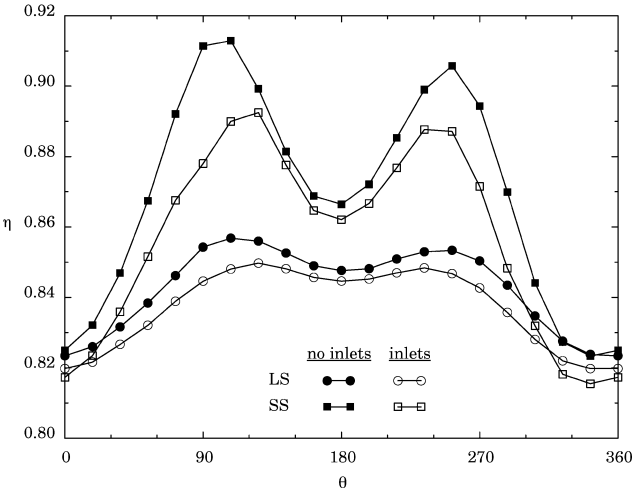

Fig. 9 SBE: GT3, $V_\infty = 130$ KIAS, 5000 ft, QCS04, 2450 rpm.

contained the QCS04 blade and the aft blade row contained the GT3 fuselage. The simulated design cruise condition for the GT3 was a flow velocity of 130 KIAS at a simulated altitude of 5000 ft with the propeller operating at 2450 rpm. The grid sizes were $99 \times 53 \times 120$ for the forward row and $99 \times 53 \times 120$ for the aft row. A slightly increased grid density was chosen for the QCS04 due to greater geometric complexity of the blade shape and the anticipated higher blade loading. The blade twist distribution was the same for both the short spinner (SS) and the long spinner (LS) configurations. For the LS case, an additional blade row of dimension 20 $\times 53 \times 120$ was

added to fill the space around the extended spinner, which shifted the QCS04 prop forward (away from the cowl) 8 in.

Again, a comparison was made by sampling the data periodically as the prop rotated from $\theta = 0$ deg through one complete clockwise revolution. Figure 9 shows the single-blade efficiency (SBE) and highlights the role of the fuselage in increasing the blade efficiency. The fuselage behaves somewhat like a ground plane, and thus, the blade behaves much like a wing in ground effect, which is known to increase effectiveness. The difference in this situation is that the pressure is also being elevated on the fuselage engine cowl, which may have a detrimental effect on the overall vehicle drag. The average efficiency of the QCS04 configuration(s) is notably higher than that of the McCauley propeller.

To demonstrate the significant variation in flow angle seen by the blade, consider Figs. 10 and 11, which show the angle of attack of the flow relative to the local chord line of the blade for the configurations

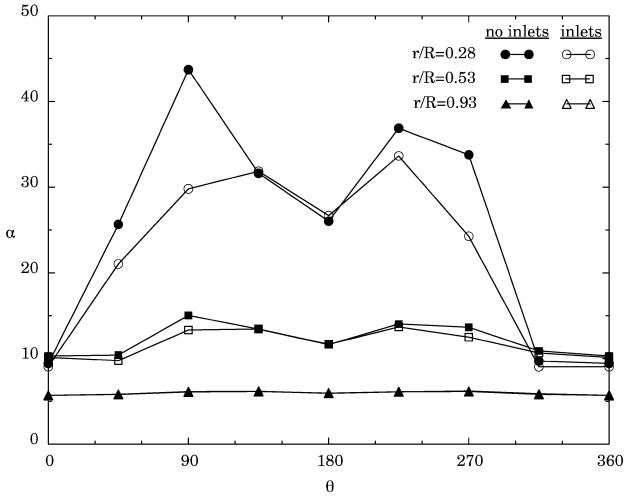

Fig. 10 Time-dependent blade-relative angle of attack, SS: GT3, V_∞ = 130 KIAS, 5000 ft, QCS04, 2450 rpm.

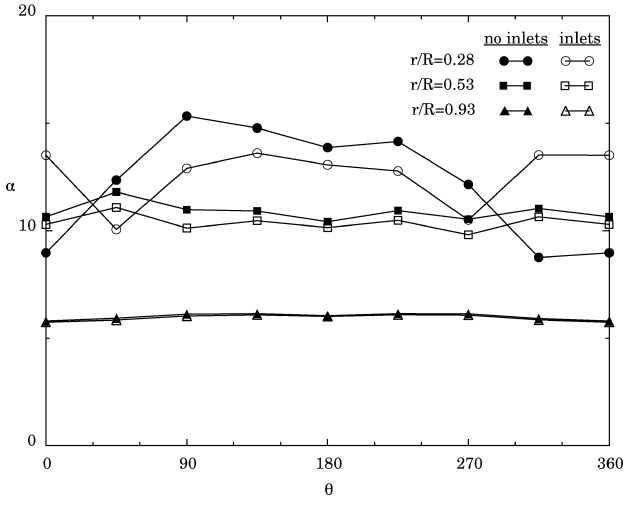

Fig. 11 Time-dependent blade-relative angle of attack, LS: GT3, V_∞ = 130 KIAS, 5000 ft, QCS04, 2450 rpm.

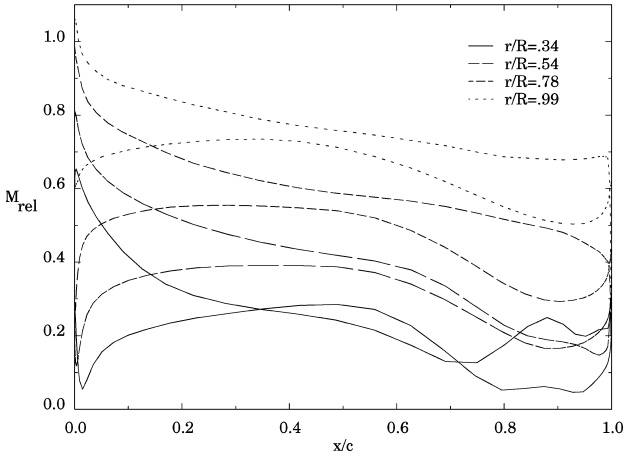

Fig. 12 Blade-relative Mach number, SS inlets: GT3, V_∞ = 130 KIAS, 5000 ft, QCS04 (θ = 90 deg) 2450 rpm.

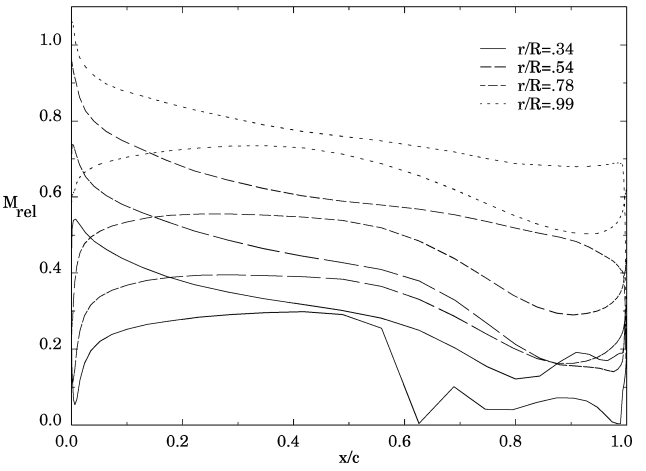

Fig. 13 Blade-relative Mach number, LS inlets: GT3, V_∞ = 130 KIAS, 5000 ft, QCS04 (θ = 90 deg) 2450 rpm.

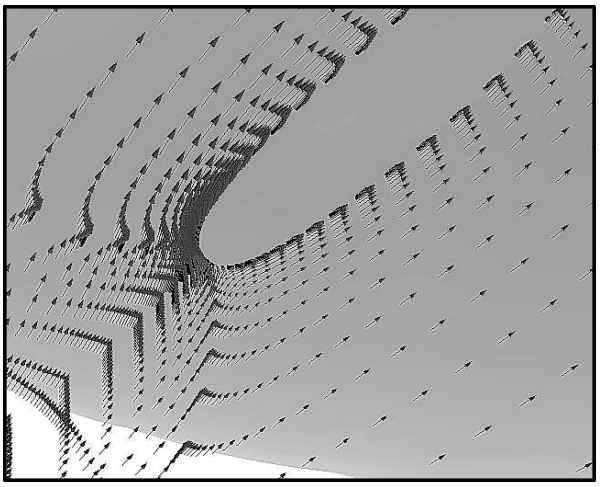

a) Blade leading-edge closeup

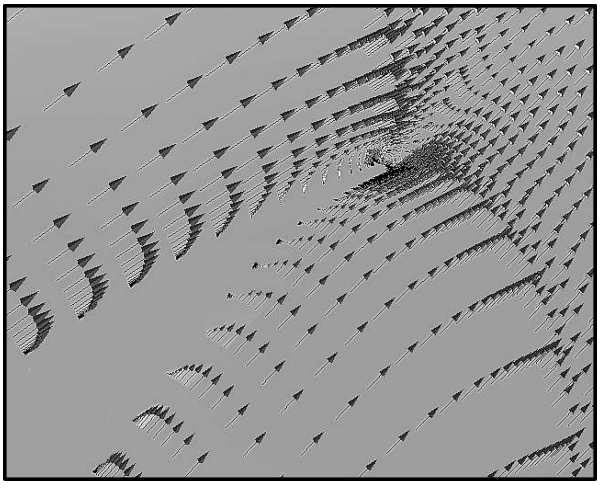

b) Blade trailing-edge closeup

Fig. 14 Blade-relative velocity vectors, LS no inlets, r/R = 0.3, $\alpha \sim$ 15 deg.

with and without cooling inlets. In the vicinity of the fuselage, the blade-relative angle of attack is shown to vary significantly. The flow angle used to calculate the blade-relative angle of attack displayed here was again taken at a location outside the boundary layer roughly normal to the local surface at the forwardmost stagnation point.

In Figs. 12 and 13, the local blade-relative Mach number is shown for selected stations on the blade. Interestingly, the flow appears to separate on the aft section of the pressure surface for the blade section near the root ($r/R = 0.34$) for the LS case. This apparent separation is confirmed by looking at the velocity vectors shown in Fig. 14. A separated region is noted near the cusped portion of the pressure surface.

The SS case, shown in Fig. 15, does not indicate the same flow separation along the cusped portion of the pressure surface; rather separation appears on the suction surface very near the trailing edge. These flowfield snapshots were generated with the propeller in the horizontal ($\theta = 90$ deg) position.

Next a numerical probe was introduced, sampling the total pressure at a location within each inlet. The analysis shows the spinner length also affects the flow through the cooling inlets. The variations in total pressure shown in Fig. 16 indicate that the left and right cooling inlets "see" a different incoming flow due to the vertical asymmetries of the geometry, and thus, the cooling of the left and right banks of cylinders will not be equal. The LS configuration does show a more uniform inflow condition for both the left and right cooling inlets. The bold line in Fig. 16 indicates the freestream stagnation pressure.

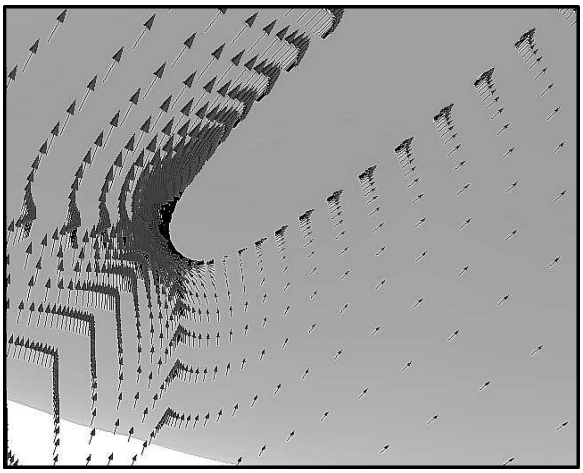

a) Blade leading-edge closeup

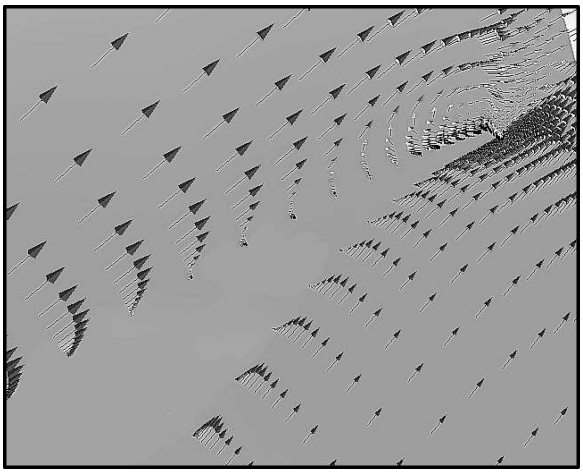

b) Blade trailing-edge closeup

Fig. 15 Blade-relative velocity vectors, SS no inlets, $r/R = 0.3$, $\alpha \sim 43$ deg.

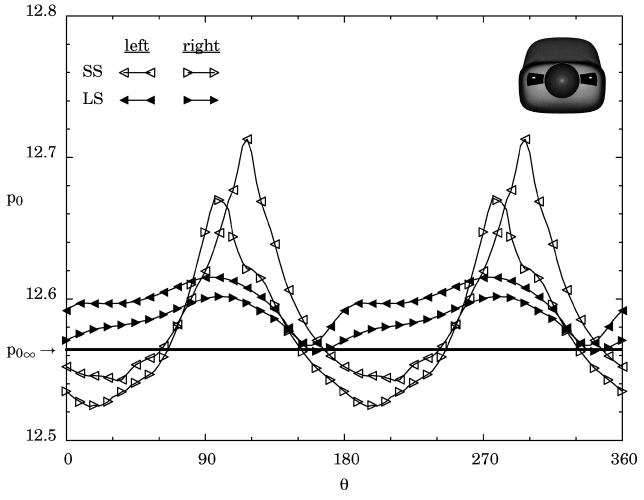

Fig. 16 Cooling inlet total pressure time history: GT3, $V_\infty = 130$ KIAS, 5000 ft, QCS04, 2450 rpm.

Conclusions

Flowfield simulations have been performed to assess the installed performance of some general aviation propellers. The configurations modeled involve the two-bladed propellers, McCauley and QCS04. The fuselage of a general aviation trainer aircraft (with and without cooling inlets) and a body of revolution hub assembly derived from the equivalent cross-sectional area of the aircraft cowl were also incorporated into the geometries studied. The simulation solutions were obtained using PROPS, a derivative of software originally developed for NASA John H. Glenn Research Center at Lewis Field. Time-dependent blade efficiency plots along with blade-relative inflow angle and velocity vector plots have provided insight toward understanding some of the mutual interference associated with the installed performance of the configurations. Numerical solutions indicate the McCauley propeller operates at a negative angle of attack near the blade root, thus, producing a reduction in efficiency. In contrast, the QCS04 blade appears to be twisted such that the root section benefits from the interference associated with the downstream fuselage structure. This beneficial effect appears to be somewhat analogous to a wing in ground effect; thus, the local lift to drag ratio (or thrust to torque ratio) increases, presenting a seemingly more efficient propeller. By design, the twist distribution of the QCS04 blade appears to be better suited to the cruise inflow angle, producing a nearly constant ~10 deg angle of attack from root to tip.

Acknowledgments

The author would like to thank the Mississippi Center for Supercomputing Research for providing extensive CPU time on their facilities to complete the simulations presented here and would like to thank Global Aircraft Corporation for providing geometry data and subcontract funding for this project.

References

[1]Janus, J. M., "Advanced 3-D CFD Algorithm for Turbomachinery," Ph.D. Dissertation, Dept. of Aerospace Engineering, Mississippi State Univ., Mississippi State, MS, May 1989.

[2]Chen, J. P., "Unsteady Three-Dimensional Thin-Layer Navier Stokes Solutions for Turbomachinery in Transonic Flow," Ph.D. Dissertation, Dept. of Aerospace Engineering, Mississippi State Univ., Mississippi State, MS, Dec. 1991.

[3]Whitfield, D. L., Swafford, T. W., Janus, J. M., Mulac, R. A., and Belk, D. M., "Three-Dimensional Unsteady Euler Solutions for Propfans and Counter-Rotating Propfans in Transonic Flow," AIAA Paper 87-1197, June 1987.

[4]Janus, J. M., and Whitfield, D. L., "A Simple Time-Accurate Turbomachinery Algorithm with Numerical Solutions of an Uneven Blade Count Configuration," AIAA Paper 89-0206, Jan. 1989.

[5]Janus, J. M., and Whitfield, D. L., "Counter-Rotating Propfan Simulations Which Feature a Relative-Motion Multiblock Grid Decomposition Enabling Arbitrary Time Steps," AIAA Paper 90-0687, Jan. 1990.

[6]Janus, J. M., Horstman, H. Z., and Whitfield, D. L., "Unsteady Flowfield Simulation of Ducted Prop-Fan Configurations," *Journal of Propulsion and Power*, Vol. 15, No. 1, 1999, pp. 264–267.